Journal of Hydrology 600 (2021) 126499

Contents lists available at ScienceDirect

Journal of Hydrology

journal homepage: www.elsevier.com/locate/jhydrol

Research papers

Spatial-temporal multivariate semi-Bayesian hierarchical framework for extreme precipitation frequency analysis

Álvaro Ossandón [a,b,*], Balaji Rajagopalan [a,c], William Kleiber [d]

[a] Department of Civil, Environmental and Architectural Engineering, University of Colorado, Boulder, CO, USA
[b] Departamento de Obras Civiles, Universidad Técnica Santa María, Valparaíso, Chile
[c] Cooperative Institute for Research in Environmental Sciences, University of Colorado, Boulder, CO, USA
[d] Department of Applied Mathematics, University of Colorado, Boulder, CO, USA

ARTICLE INFO

Keywords:
Spatial extremes
Semi-Bayesian hierarchical Modeling
Nonstationary model of extremes
Southwest US summer precipitation extremes

ABSTRACT

We present a semi-Bayesian hierarchical modeling framework for conducting space–time frequency analysis of precipitation extremes over a large domain. In this framework, the data layer, the precipitation extreme – i.e., seasonal maximum precipitation, at each station in each year is modeled using a generalized extreme value (GEV) distribution with temporally varying parameters, which are decomposed as linear functions of covariates. The coefficients of the covariates are estimated via maximum likelihood (ML). In the process layer, the estimated ML coefficients of each of the covariates across the stations are spatially modeled with a Gaussian multivariate process which enables capturing the spatial structure and correlation between the spatial model parameters. Suitable priors are used for the spatial model hyperparameters to complete the Bayesian formulation. Since the Bayesian formulation is only at the second level, our model is semi-Bayesian and thus, the posteriors are conditional posterior distributions. With the conditional posterior distribution of spatial fields of the GEV parameters for each time, conditional posterior distribution of the nonstationary space–time return levels of the precipitation extremes are obtained. We demonstrate this framework by application to summer precipitation extreme at 73 stations covering a large domain of Southwest US consisting of Arizona, New Mexico, Colorado, and Utah. The results from fitting and cross-validation indicate that our model captures the historical variability at the stations very well. Conditional posterior distributions of return levels are simulated on a grid over the domain, which will be of immense utility in management of natural resources and infrastructure.

1. Introduction

Extreme precipitation leads to extreme flow – i.e., flood events leading to loss of lives and severe damage to infrastructure. Thus, it is crucial for the engineering design of infrastructure, such as flood protection, dams, and management of water supply, and flood control to understand and model the variability of extreme precipitation in both space and time. A common practice is to perform frequency analysis on block (i.e. seasonal or annual) precipitation extreme using statistical distributions. A single set of distribution parameters are estimated assuming stationarity, in that the precipitation variability in the future will be similar to that of the past (Jakob, 2013). The fitted distributions are used to estimate occurrence probabilities (i.e., return period) of rare events of desired magnitudes and return levels of desired risks – all, useful in infrastructure design (Coles, 2001).

Although for modeling extreme precipitation some studies have used log-normal and Gumbel distributions (Hershfield, 1961; Wilks, 1993), the Generalized Extreme Value (GEV) distribution, which is theoretically more appropriate, is widely used (e.g., Dupuis and Field, 1998; Gellens, 2002; Wilks, 1993) due to its ability to capture a wide range of tail behaviors, and also it is consistent with extreme value theory (EVT) (Coles, 2001).

There are two main problems related to this single site stationary frequency analysis approach: the stationarity assumption may not be valid since diverse modeling and empirical studies have shown that the frequency and intensity of extreme climatic events are increasing and will continue to do in the foreseeable future due to climate variability and change (Barnett et al., 2006; Frich et al., 2002; IPCC, 2007; Milly et al., 2008; Schmidli and Frei, 2005); and the need for estimating extreme precipitation at several locations where data is not available for

* Corresponding author at: Department of Civil, Environmental and Architectural Engineering, University of Colorado, Boulder, CO, USA.
E-mail address: alvaro.ossandon@colorado.edu (Á. Ossandón).

https://doi.org/10.1016/j.jhydrol.2021.126499

Available online 31 May 2021

designing of infrastructure or hazard mitigation. These motivate the need for modeling approaches that capture the variability of extremes in space and time. Temporal variability of extremes is modeled by varying the parameters of the statistical distribution as a function of covariates by a Generalized Linear Modeling (McCullagh and Nelder, 1989) approach. An early approach for modeling the temporal variability of parameters of GEV as functions of time, was proposed in Katz et al. (2002).

This led to plethora of studies that applied this approach at individual sites with time-varying covariates besides time trend, to modeling the temporal nonstationarity of precipitation extremes around the world. As mentioned, linear time trend to model the time-varying GEV parameters is the simplest nonstationary model (Fowler et al., 2010; van Haren et al., 2013; Katz et al., 2002). Other time-varying covariates have been used to model precipitation extremes in Asia (Agilan and Umamahesh, 2017; Gao et al., 2016), North America (El Adlouni et al., 2007; Um et al., 2017), Europe (Vasiliades et al., 2015), Australia (Agilan and Umamahesh, 2016), and elsewhere.

Extensions of this in a Bayesian approach have been developed (Cannon, 2010; Cheng and Aghakouchak, 2014; Ouarda and El-Adlouni, 2011) which captures the uncertainties in the parameters and consequently in the return levels, robustly, via their posterior distributions. However, most of these studies are single-site analyses or assume spatial independence, thus, cannot provide estimates at any arbitrary ungauged location.

To address this, studies have extend extreme value analysis and other methods to model inter-site dependency. These include - regional frequency analysis such as the index-flood method (Wazneh et al., 2013); max-stable processes (Coles, 1993; Coles and Tawn, 1996; Davison et al., 2012; Stephenson et al., 2016); spatial modeling of marginal GEV parameters by univariate spatial Gaussian processes (Dyrrdal et al., 2015; Yan and Moradkhani, 2015; Yan and Moradkhani, 2016; Reza Najafi and Moradkhani, 2013); capturing the spatial dependency by both Gaussian copulas and spatial modeling of marginal GEV parameters, and quantifying uncertainties of variables by hierarchical Bayesian processes of the latent parameters (Bracken et al., 2016; Renard, 2011).

Despite these advances, limited studies have offered models for spatial and temporal nonstationarity of climate extremes, especially precipitation extremes. Hanel et al. (2009) modeled the nonstationarity in extreme precipitation over the Rhine basin using a spatial extreme value model based on the index-flow method that divided the domain into homogeneous regions where the GEV coefficients are assumed to be constant. Lima et al. (2016) used a hierarchical Bayesian GEV model for flood quantile estimates in which spatial dependency is captured by scaling the GEV parameters independently according to their drainage area, i.e., independent normal prior distributions are considered for the GEV parameters. Other authors have used the same approach to model extreme precipitation (Apputhurai and Stephenson, 2013; Steinschneider and Lall, 2015). Ahn et al. (2017) introduced a hierarchical Bayesian model for regionalized seasonal forecasts where the spatial dependency is captured by modeling the probability distribution parameters with a multivariate Gaussian field. Bracken et al. (2018) and Sun et al. (2014) implemented a multivariate nonstationary Bayesian hierarchical model for hydrologic frequency analysis, in which the dependence between variables was captured by a Gaussian elliptical copula in the data layer. While these are very good approaches, some general issues remain - such as, limited ability to capture spatial dependencies over the entire domain if GEV parameters are kept constant over homogeneous regions; estimation issues with Copulas as the domain size increases; inability to capture relationships between the parameters as each parameter is modeled separately in space; these work well for smaller spatial domains or fewer variables, but become computationally intensive and have convergence issues as the domain increases, to name a few.

Our research in this paper is motivated by the need to address these issues and have the ability to obtain estimates of return levels and their uncertainties at ungauged locations. To this end, we propose a semi-Bayesian Hierarchical framework to model multi-site spatio-temporal variability of precipitation extremes.

We demonstrate this framework by its application to extreme summer precipitation at 73 stations from the Southwest US- Arizona, New Mexico, Colorado, and Utah. The paper is organized as follows. In Section 2, the framework, in general, is described. The application set up for the Southwest US extreme precipitation is then described, followed by the specific form of the model structure and fitting method in Section 3. The results are described in Section 4, and Section 5 presents a sumamry and discussion of the results.

2. Proposed framework

The proposed spatial–temporal multivariate semi-Bayesian hierarchical framework is comprised of three components: the model structure, the estimation strategy, and estimation of nonstationary return levels.

2.1. General model structure

In general, we wish to conduct a nonstationary frequency analysis of extreme precipitation at m locations over k years, and then use a spatial model that allows us to estimate return levels and their uncertainty over a grid or at stations with missing data. In this context, it is assumed that extreme precipitation series at each station follows a GEV distribution (Coles, 2001; Katz, 2013). The spatial dependence is captured through a spatial multivariate Gaussian process on the GEV parameters. The first layer of the hierarchical model structure, also known as the data layer, corresponds to the GEV distribution assumed at each location s_i and time point t which is

$$Y(s_i,t) \sim GEV(\mu(s_i,t),\sigma(s_i,t),\xi(s_i,t)), \quad i=1,\ldots,m \tag{1}$$

where $\mu \in (-\infty,\infty)$ is the location parameter, $\sigma>0$ is the scale parameter, and $\xi \in (-\infty,\infty)$ is the shape parameter. Under the nonstationary assumption, distribution parameters can vary in space and time. Thus, the three GEV parameters could be modeled as functions of time-dependent large-scale climate variables, and regional mean covariates:

$$\mu(s_i,t) = \alpha_{\mu 0}(s_i) + \sum_{j=1}^{n} \alpha_{\mu j}(s_i) Z_j(t), \quad i=1,\ldots,m \tag{2}$$

$$\log(\sigma(s_i,t)) = \alpha_{\sigma 0}(s_i) + \sum_{j=1}^{n} \alpha_{\sigma j}(s_i) Z_j(t), \quad i=1,\ldots,m \tag{3}$$

$$\xi(s_i,t) = \alpha_{\xi 0}(s_i) + \sum_{j=1}^{n} \alpha_{\xi j}(s_i) Z_j(t), \quad i=1,\ldots,m \tag{4}$$

where $\alpha_\mu, \alpha_\sigma$, and α_ξ are the regression coefficients, and $Z_j(t)$ is covariate j at the time t. $\log(\sigma)$ is modeled to ensure positive scale parameters. The regression coefficients are estimated using Maximum Likelihood (ML) approach (Katz et al., 2002). Specific choices for covariates in our data analysis will be discussed in Section 3.2.

While in many studies, ξ is modeled as a single value per study area or per region within the study area (Apputhurai and Stephenson, 2013; Atyeo and Walshaw, 2012; Cooley et al., 2007; Renard, 2011), others consider that this parameter varies spatially along with the other GEV parameters, but considering a specific range of variation for it (Bracken et al., 2016; Cooley and Sain, 2010). Here, because we are interested in capturing the correlation between GEV parameters, no a priori restriction on its domain is imposed.

The Bayesian formulation starts in the process layer, which is the second layer of the hierarchy, assumes a multivariate spatial Gaussian process for the GEV regression coefficients obtained via ML as

mentioned above. Compared to a univariate spatial Gaussian process (e.g., Yan and Moradkhani, 2015; Sun et al., 2014), this process can account for cross-correlation in the regression coefficients. The covariates selected for modeling the GEV parameters in the first level exhibit spatial correlation, thus, the GEV regression coefficients are likely to be correlated. Therefore, the multivariate spatial Gaussian Process formulation is appropriate and general, regardless of the strength of the spatial correlation. Thus, the GEV regression coefficients at the location s_i are modeled as

$$\boldsymbol{\alpha}(s_i) = \boldsymbol{\beta}^T \mathbf{X}(s_i) + \mathbf{w}(s_i) + \epsilon(s_i) \tag{5}$$

where $\boldsymbol{\alpha}(s_i) = [\boldsymbol{\alpha}_\mu(s_i), \boldsymbol{\alpha}_\sigma(s_i), \boldsymbol{\alpha}_\xi(s_i)]$ is a vector of $3(n+1) \times 1$ GEV regression coefficients at the location s_i; $\boldsymbol{\beta} = [\boldsymbol{\beta}_\mu, \boldsymbol{\beta}_\sigma, \boldsymbol{\beta}_\xi]$ is a matrix of $4 \times 3(n+1)$ spatial regression coefficients which are constant in space and time; $\mathbf{X}(s_i)$ is a 4×1 vector of regressors with the elements corresponding to the unity, coordinates, and elevation at the location s_i; and $\mathbf{w}(s_i)$ and $\epsilon(s_i)$ are vectors of $3(n+1) \times 1$ spatial and uncorrelated residuals at location s_i, respectively. We assume the parameters can be defined through a latent multivariate process comprised of two components: a spatial term, $\mathbf{w}$, that follows a mean 0, stationary, anisotropic Gaussian process specification with a covariance function C, and independent white-noise process, ϵ.

Considering m locations, we have that spatial and uncorrelated residuals are

$$\mathbf{w} = [\mathbf{w}(s_1), \mathbf{w}(s_2), \ldots, \mathbf{w}(s_m)]^T \tag{6}$$

$$\epsilon = [\epsilon(s_1), \epsilon(s_2), \ldots, \epsilon(s_m)]^T \tag{7}$$

The spatial residuals vector, $\mathbf{w}$, follows a $MVN(0, \boldsymbol{\Sigma}_s)$, where $\boldsymbol{\Sigma}_s$ is the $mp \times mp$ covariance matrix and $p = 3(n+1)$. The covariance matrix is defined as

$$\boldsymbol{\Sigma}_s = \begin{bmatrix} \mathbf{C}_{11} & \cdots & \mathbf{C}_{1p} \\ \vdots & \ddots & \vdots \\ \mathbf{C}_{p1} & \cdots & \mathbf{C}_{pp} \end{bmatrix} \tag{8}$$

where $\mathbf{C}_{kl}$ is a $(m \times m)$ cross-covariance matrix. When $k = l$, it corresponds to a covariance matrix. We consider an exponential covariance function with parameters δ_{kl}^2 (the partial sill or marginal variance), ϕ_{kl} (the spatial decay parameter). The parametric form of the covariance and cross-covariance functions is

$$C_{kl}(s_i, s_j) = \delta_{kl}^2 \exp\left(-\phi_{kl} \|s_i - s_j\|\right) \tag{9}$$

This specification is a particular type of multivariate Matérn (Gneiting et al., 2010); there are some restrictions on parameters that result in a valid, i.e., nonnegative definite covariance matrix, see Gneiting et al. (2010) or Apanasovich et al. (2012) for details.

For the uncorrelated residuals, we have $\epsilon \sim MVN(0, \boldsymbol{\Sigma}_{ns})$, where $\boldsymbol{\Sigma}_{ns}$ is $mp \times mp$ diagonal covariance matrix

$$\boldsymbol{\Sigma}_{ns} = \begin{bmatrix} \tau_1^2 \mathbf{I} & 0 & \cdots & 0 \\ 0 & \tau_2^2 \mathbf{I} & \cdots & 0 \\ \vdots & \vdots & \ddots & \vdots \\ 0 & 0 & \cdots & \tau_p^2 \mathbf{I} \end{bmatrix} \tag{10}$$

where τ_k^2 is the nugget effect related to the kth GEV regression coefficient, and $\mathbf{I}$ is a $(m \times m)$ identity matrix.

A conceptual sketch of the spatial–temporal multivariate semi-Bayesian hierarchical framework is shown in Fig. 1 which shows the data layer (maximum likelihood estimation of the GEV regression coefficients) and the process layer (multivariate spatial Gaussian process for the GEV regression coefficients obtained in the data layer).

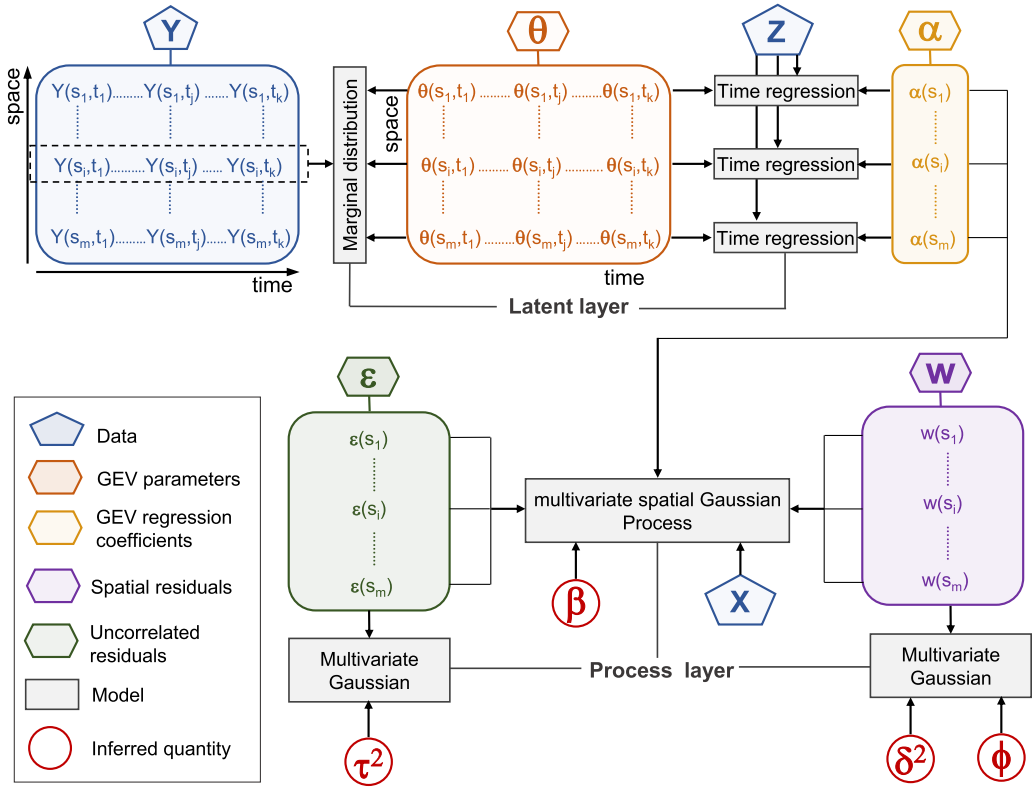

Fig. 1. Conceptual sketch of the spatial–temporal multivariate semi-Bayesian hierarchical framework. $\boldsymbol{\theta}(s_i, t_j) = [\boldsymbol{\mu}(s_i, t_j), \log\boldsymbol{\sigma}(s_i, t_j), \boldsymbol{\xi}(s_i, t_j)]$.

2.2. Estimation strategy

First, GEV regression coefficients of the data layer are estimated from Eqs. (1)–(4) using maximum likelihood. Then, the conditional posterior distribution of the spatial regression coefficients, $\boldsymbol{\beta}$, and residuals parameters, $\boldsymbol{\delta}^2, \boldsymbol{\phi}, \boldsymbol{\tau}^2$, given maximum likelihood estimates (MLEs) of the GEV regression coefficients, $\widehat{\boldsymbol{\alpha}}$, which are assumed as the true values of the GEV regression coefficients, and spatial regressors $\mathbf{X}$, are obtained using the multivariate Bayesian model. By Bayes' rule, the posterior distribution is

$$p(\boldsymbol{\beta},\mathbf{w},\boldsymbol{\delta}^2,\boldsymbol{\phi},\boldsymbol{\tau}^2|\widehat{\boldsymbol{\alpha}},\mathbf{X}) \propto p(\widehat{\boldsymbol{\alpha}}|\boldsymbol{\beta},\mathbf{w},\boldsymbol{\delta}^2,\boldsymbol{\phi},\boldsymbol{\tau}^2,\mathbf{X})\cdot p(\boldsymbol{\beta},\mathbf{w},\boldsymbol{\delta}^2,\boldsymbol{\phi},\boldsymbol{\tau}^2|\mathbf{X}) = p(\widehat{\boldsymbol{\alpha}}|\boldsymbol{\beta},\mathbf{w},\boldsymbol{\tau}^2,\mathbf{X})\cdot p(\mathbf{w},\boldsymbol{\delta}^2,\boldsymbol{\phi})\cdot p(\boldsymbol{\tau}^2)\cdot p(\boldsymbol{\beta}) = p(\widehat{\boldsymbol{\alpha}}|\boldsymbol{\beta},\mathbf{w},\boldsymbol{\tau}^2,\mathbf{X})\cdot p(\mathbf{w}|\boldsymbol{\delta}^2,\boldsymbol{\phi})\cdot p(\boldsymbol{\delta}^2)\cdot p(\boldsymbol{\phi})\cdot p(\boldsymbol{\tau}^2)\cdot p(\boldsymbol{\beta}) \tag{11}$$

here term $p(\mathbf{w}|\boldsymbol{\delta}^2,\boldsymbol{\phi}) = f_{MVN}(\mathbf{w}|\mathbf{0},\boldsymbol{\Sigma}_s)$; $f_{MVN}(\mathbf{w}|\mathbf{0},\boldsymbol{\Sigma}_s)$ represents the probability density of a multivariate normal distribution with mean $\mathbf{0}$ and covariance $\boldsymbol{\Sigma}_s$ (see Eq. 8); $p(\boldsymbol{\beta}) = f_{MVN}(\boldsymbol{\beta}|\boldsymbol{\mu}_\beta,\boldsymbol{\Sigma}_\beta)$; $\boldsymbol{\mu}_\beta$ and $\boldsymbol{\Sigma}_\beta$ are the spatial regression coefficient estimates and their covariance matrix obtained from a linear model fitting (Eq. 5) using maximum likelihood; $p(\boldsymbol{\delta}^2)$, $p(\boldsymbol{\phi})$, and $p(\boldsymbol{\tau}^2)$ are the priors of the other parameters, which based on Finley et al. (2015) are assumed to be independent and follow the following distributions

$$\boldsymbol{\delta}^2 \sim invWishart(\nu,\mathbf{S}),\quad \boldsymbol{\phi} \sim Unif(\mathbf{l}_l,\mathbf{u}_l),\quad \boldsymbol{\tau}^2 \sim InvGamma(\boldsymbol{\kappa},\boldsymbol{\gamma}) \tag{12}$$

where ν and $\mathbf{S}$ are the degrees of freedom and scale matrix of the inverse-Wishart distribution; $\boldsymbol{l}_l$ and $\boldsymbol{u}_l$ are the lower and upper limits vectors of the uniform distribution; $\boldsymbol{\kappa}$ and $\boldsymbol{\gamma}$ are the shape and scale hyperparameters vectors of the inverse-Gamma distribution. The term $p(\widehat{\boldsymbol{\alpha}}|\boldsymbol{\beta},\mathbf{w},\boldsymbol{\tau}^2,\mathbf{X})$ is the likelihood of MLEs of the GEV regression coefficients, $\widehat{\boldsymbol{\alpha}}$, conditional on the dependence of the uncorrelated residuals, the regression coefficients $\boldsymbol{\beta} = [\boldsymbol{\beta}_\mu,\boldsymbol{\beta}_\sigma,\boldsymbol{\beta}_\xi]$, and spatial residuals. The likelihood of $\widehat{\boldsymbol{\alpha}}$ is defined as a multivariate normal

$$p(\widehat{\boldsymbol{\alpha}}|\boldsymbol{\beta},\mathbf{w},\boldsymbol{\tau}^2,\mathbf{X}) = f_{MVN}(\widehat{\boldsymbol{\alpha}}|\mathbf{X}^T\boldsymbol{\beta}+\mathbf{w},\boldsymbol{\Sigma}_{ns}) \tag{13}$$

where $\mathbf{X}$ is a known $m \times p$ matrix of spatial regressors.

2.3. Nonstationary return levels

According to Read and Vogel (2015), it is important to be clear when discussing nonstationary return levels and return periods since there are several definitions (Cheng et al., 2014; Salas and Obeysekera, 2014; Katz, 2013). For a stationary GEV distribution the return level, T, is defined as the $p = (1-1/T)$th quantile

$$q_p = \mu + \frac{\sigma}{\xi}[(-\log p)^{-\xi} - 1] \tag{14}$$

Here, we use the definition for nonstationary return levels provided by Cheng et al. (2014), which states that in a nonstationary setting when the GEV parameters may be time-varying, the return level can be computed at each year, which is known as the effective return level

$$q_p(t) = \mu(t) + \frac{\sigma(t)}{\xi(t)}[(-\log p)^{-\xi(t)} - 1] \tag{15}$$

3. Application

The Southwest US region comprising of the four states -Arizona, New Mexico, Colorado, and Utah- is the hottest and driest region of the United States. Most of the precipitation arrives during the winter season, but the summer precipitation makes a significant contribution to the reliability of water resources and the health of ecology. However, summer precipitation and its extremes, over this region exhibit a high degree of spatial and temporal variability (Sheppard et al., 2002). We demonstrate the utility of our proposed framework presented in the previous section by its application to summer precipitation extremes at 73 stations from this region.

3.1. Precipitation data

Daily summer, June through September, precipitation data were obtained from the Global Historical Climatology Network (GHCN) (Menne et al., 2012). We selected stations with a full record of data for the period 1964 to 2018 or those with no more than 10% of data missing or no more than three years of missing data in a row. This resulted in 73 stations for which climatology of the extreme seasonal precipitation is shown in Fig. 2 along with an elevation grid. Summer season 3-day maximum precipitation was computed for each year at each station. For a station with missing year values, these values were substituted with the median value of the station.

3.2. Covariates

Some studies (Higgins et al., 1999; Mamalakis et al., 2018; McCabe et al., 2004) have shown that there is a weak statistical relationship between Southwest US summer precipitation and large-scale climate indices capturing drivers in tropical Pacific - El Nino Southern Oscillation (ENSO), Northern Pacific – Pacific Decadal Oscillation (PDO), and Atlantic – Atlantic Multidecadal Oscillation (AMO). Since our objective is to demonstrate our framework, we rely on these prior researches, and considered these large-scale climate indices as potential covariates, albeit with a somewhat weaker association, for the nonstationary GEV distribution in the framework. However, users can develop tailored covariates for their specific data to enhance model performance.

For modeling the temporal nonstationarity of the GEV parameters (see Eqs. (2)–(4)), first, we considered summer season average ENSO and PDO indices, and the standardized spatial average of summer seasonal precipitation (SASP) over the entire region as potential covariates. We obtained values of the multivariate ENSO index (MEI) (Wolter and Timlin, 1993; Wolter and Timlin, 1998; Wolter and Timlin, 2011) from http://www.esrl.noaa.gov/psd/enso/mei/. The PDO values (Zhang et al., 1997) were obtained from http://research.jisao.washington.edu/pdo/. The average summer season precipitation, SASP, was computed from the GHCN (Menne et al., 2012).

We assess the strength of the relationship between the covariates and the summer precipitation extreme by computing the Spearman's rank correlations, shown in Fig. 3. It can be seen that SASP exhibits significant correlation with summer precipitation extreme across at almost all the locations over the domain. However, ENSO and PDO indices present a weaker correlation with precipitation extremes and significant at only few locations. Previous studies mentioned earlier in this section investigated relationship between these indices and seasonal total precipitation in this region and found them to stronger. But, from our analysis, the indices ride a weaker signature on the precipitation extremes. We selected the best nonstationary GEV model using total Akaike information criteria (AIC) (Akaike, 1974) and total Bayesian information criterion (BIC) (Schwarz, 1978). In this, the nonstationary model is fitted to the precipitation extreme at each location and the AIC and BIC values of all the individual location models are added to obtain the total AIC and

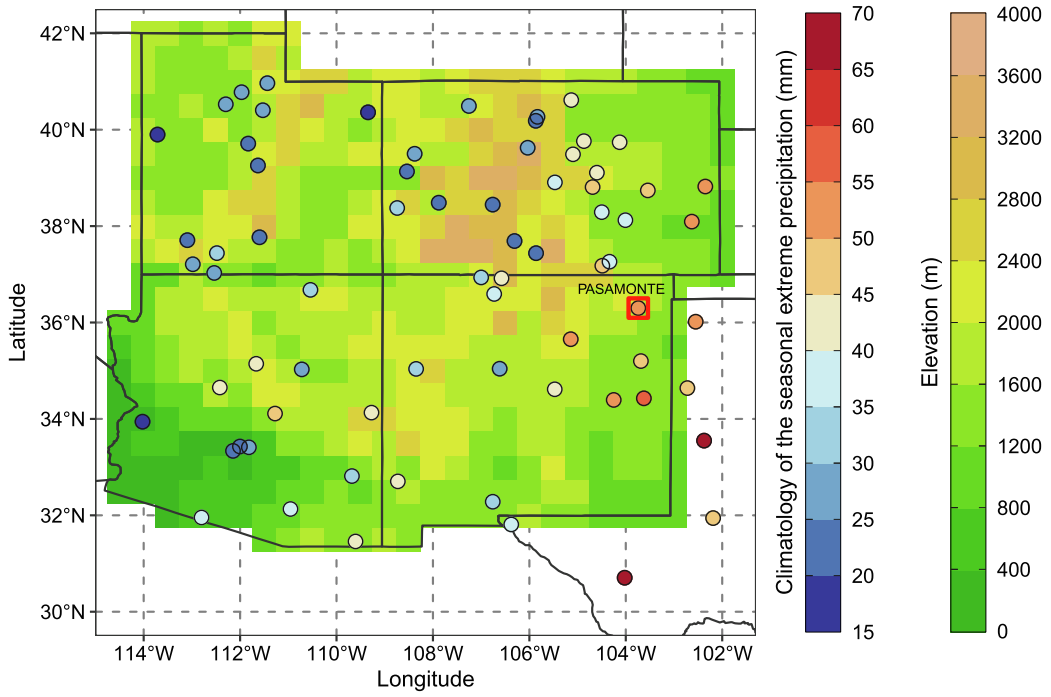

Fig. 2. Climatology of the extreme seasonal precipitation for 73 precipitation stations and 0.5-degree elevation grid in (m) of the study area. The red square corresponds to the site of interest, considered in Section 4.

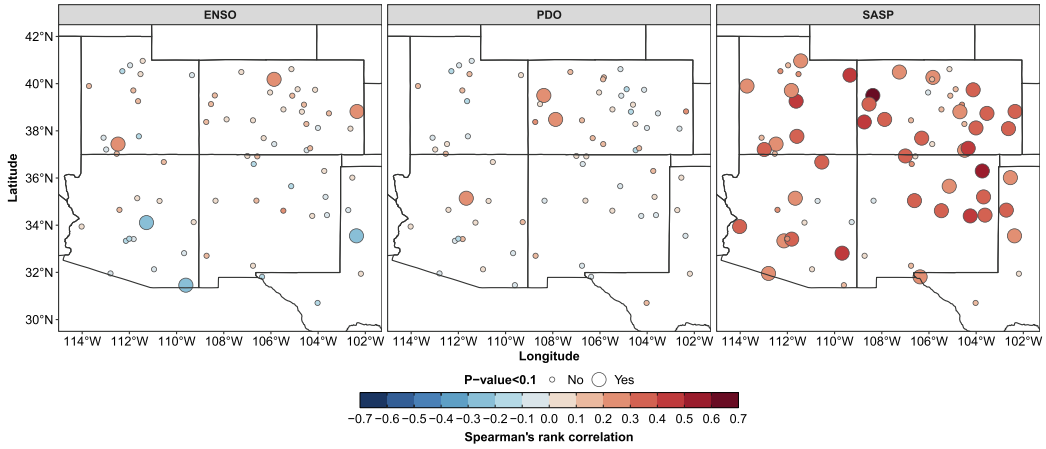

Fig. 3. Spearman's rank correlation coefficient between summer 3-day maximum precipitation and covariates: (left column) ENSO; (middle column) PDO; (right column) the standardized spatial average of seasonal total precipitation. Big circles indicate that the Spearman's rank correlation is significant (P-value<0.1).

BIC values. These are computed for a suite of candidate models with various combinations of the covariates and the model with the minimum total AIC or BIC is selected.

For modeling the GEV regression coefficients spatially, we included covariates of latitude, longitude, and elevation. Covariates were obtained at station locations and a 0.5-degree grid throughout the study area. We obtained the elevation data from the NASA Land Data Assimilation Systems (NLDAS) (Xia et al., 2012) (https://ldas.gsfc.nasa.gov/nldas/elevation).

3.3. Model structure for the Southwest US

For the structure of the model for the Southwest US, we incorporated the above covariates for spatial and temporal modeling. We model the location and scale parameters of the GEV at each location, nonstationary. Shape parameters are generally more variable, leading to convergence issues in ML estimation, thus, most studies in literature generally keep this stationary. Following this, the shape parameter was keep stationary at each location. Based on both, the total AIC and BIC values, shown in Table 1, the best model selected uses only SASP as

Table 1
Total AIC and BIC values for different sets of covariates. for each case the same covariates are considered for location and scale parameters, and the shape parameter is considered stationary.

Covariates	AIC	BIC
ENSO	33856.7	34589.4
PDO	33858.9	34591.5
SASP	33529.0	34261.7
ENSO, PDO	33977.4	35003.2
ENSO, SASP	33657.7	34683.5
PDO, SASP	33672.4	34698.2
ENSO, PDO, SASP	33672.4	34698.2

covariate to model the location and scale parameters. The next best model, though, includes ENSO. The priors on the spatial regression coefficients and residuals parameters used are:

$$\begin{aligned} \boldsymbol{\beta} &\sim MVN(\boldsymbol{\mu}_\beta, \boldsymbol{\Sigma}_\beta)\ \boldsymbol{\delta}^2 \sim invWishart(\nu, \mathbf{S}) \\ \boldsymbol{\phi} &\sim Unif(\mathbf{l}_l, \mathbf{u}_l) \quad \boldsymbol{\tau}^2 \sim InvGamma(\boldsymbol{\kappa}, \boldsymbol{\gamma}) \end{aligned} \tag{16}$$

where $\boldsymbol{\beta}(s_i) = [\boldsymbol{\beta}_\mu, \boldsymbol{\beta}_\sigma, \boldsymbol{\beta}_\xi]$, $\boldsymbol{\mu}_\beta$ and $\boldsymbol{\Sigma}_\beta$ are the spatial regression coefficient estimates and their covariance matrix obtained from a linear model fitting (Eq. 5) on the maximum likelihood estimates of $\boldsymbol{\alpha}$, for each GEV regression coefficient separately. Based on the recommendations from Banerjee et al. (2004) and Cooley et al. (2007), informative priors were considered for the spatial residuals parameters, $\boldsymbol{\phi}$, $\boldsymbol{\delta}^2$, and non-informative priors were considered for the uncorrelated residuals parameters, $\boldsymbol{\tau}^2$. We set hyperparameter values of $\boldsymbol{\phi}$ as $\boldsymbol{l}_l = [0.2]_{6\times1}$, $\boldsymbol{u}_l = [14]_{6\times1}$, which corresponds to the range of distances for the domain considered here.

For $\boldsymbol{\delta}^2$, we set the priors based on sample variograms from the predicted residuals obtained from the linear model fitting on the maximum likelihood estimates of $\widehat{\boldsymbol{\alpha}}$, along with a exponential model which is consistent with the covariance and cross-covariance functions considered here (for more details see Cressie, 1993). Sample variograms are shown in Fig. 4. Thus, based on the exponential models fitted to the variograms, we considered the diagonal of the matrix $\mathbf{S}$, which is (5×5) matrix, equal to $[36, 5, 0.06, 0.05, 0.3]$ and $\nu = 6$ (number of rows of $\mathbf{S}$ plus 1). Finally, we set the hyperpameter values of $\boldsymbol{\tau}^2$ as $\boldsymbol{\kappa} = [1]_{6\times1}$ and $\boldsymbol{\gamma} = [0.01]_{6\times1}$.

Note that the priors of both spatial regression coefficients and spatial residuals are assumed to be independent. We expect the model capture the correlation in these parameters if it exists in the posterior. This would not be possible with univariate spatial Gaussian process. Since the Bayesian formulation is only at the second level with the spatial model of the ML estimates, our model is semi-Bayesian and thus, the posteriors are conditional posterior distributions. With the conditional posterior distribution of spatial fields of the GEV parameters for each time, conditional posterior distribution of the nonstationary space–time return levels of the precipitation extremes are obtained.

3.4. Implementation and model fitting

The model was implemented in R using the extRemes package (Gilleland and Katz, 2016) for the data layer and the spBayes package (Finley et al., 2015) for the process layer. The parameters of the nonstationary GEV parameters at each location were estimated via maximum likelihood. The spatial Bayesian multivariate model was fit using a Markov Chain Monte Carlo (MCMC) method, specifically, Gibbs sampling and random walk Metropolis steps (Robert and Casella, 2004). One chain of length 120,000 was run, with the first 60,000 iterations discarded as warmup, and a sample thinning factor of 12, resulting in 5000 samples for each parameter. To assess convergence, trace plots were visually inspected, and also a Metropolis sampling acceptance percent above 80% was checked.

3.5. Computation of return levels

With the model fitted from the steps above, posterior distributions of each GEV parameter for each year are obtained at station locations or on the 0.5-degree grid by evaluating Eqs. (2)–(5). Thus, generated parameter values are used to compute nonstationary return levels at each station or grid point using Eq. (15). The steps for this procedure are as follows:

1. Select a single conditional posterior sample of all model parameters $(\boldsymbol{\beta}, \boldsymbol{\delta}^2, \boldsymbol{\phi}, \boldsymbol{\tau}^2)$.
2. Simulate spatial and nonspatial residuals, $\mathbf{w}$ and ϵ.
3. Compute regression coefficients for GEV parameters, Eq. (5).
4. Compute GEV parameters at each location i and year t, Eqs. (2)–(4).
5. Compute nonstationary return levels at each location i and year t, Eq. (15).
6. Repeat steps 1–5 for each posterior sample.

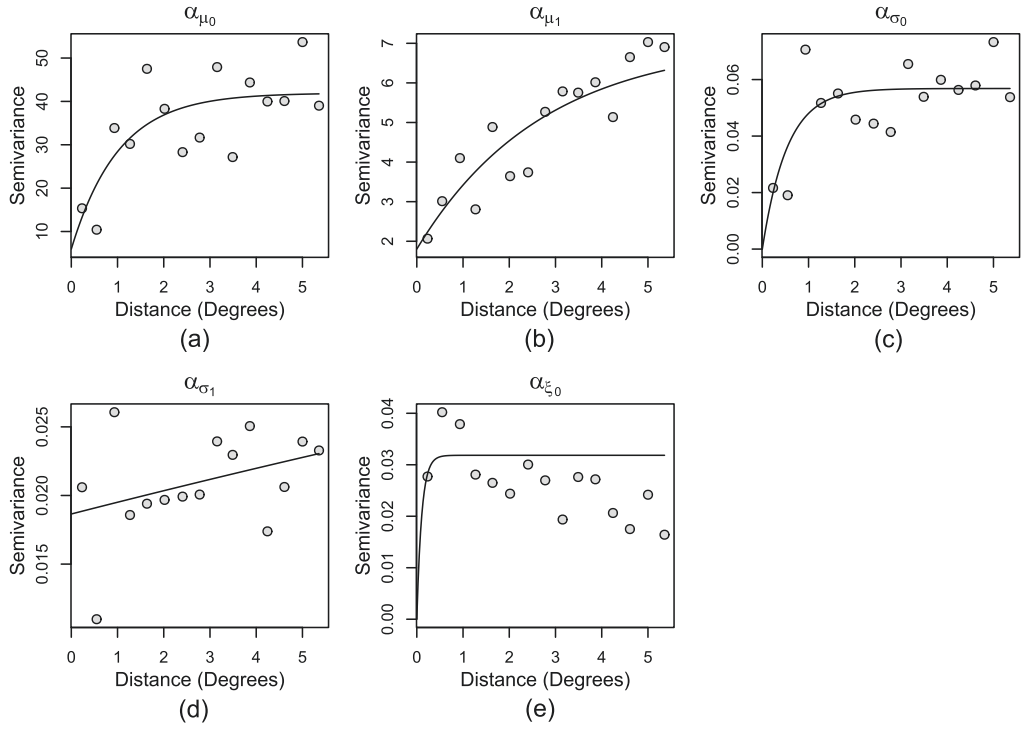

Fig. 4. Sample variograms from the predicted residuals obtained from the linear model fitting on the maximum likelihood estimates of the GEV regression coefficients, $\boldsymbol{\alpha}$. Solid lines represent the least squares estimation of the exponential model of the variogram.

3.6. Model comparison

To highlight the advantages of our framework, we compare it with another model. The models are as follows:

1. *Semi-Bayesian univariate*: A univariate nonstationary GEV distribution is fit to each location using MLE, where the location parameter is allowed to vary over time according to covariates specified in Section 3.2. Then, the spatial dependence is captured through a spatial univariate Gaussian process on each GEV parameter.
2. *Semi-Bayesian multivariate*: The spatial–temporal semi-Bayesian multivariate hierarchical framework described in this study.

4. Results

4.1. Model fits

Fig. 5 shows the Q-Q plot, the empirical Probability Density Function (PDF) and the PDF of the nonstationary GEV distribution fitted, and time series of nonstationary of the MLE return levels for different return periods for the extreme summer precipitation at Pasamonte station in New Mexico (see Fig. 2). The empirical PDF in Fig. 5b is obtained by a kernel density estimator which smooths the histogram (e.g., Bowman and Azzalini, 1997). It can be seen that in general, model and sample quantiles fall close to the 1:1 line (Fig. 5a), and the fitted GEV distribution captures the shape of the empirical PDF very well (Fig. 5b). However, there is an overestimation of the upper tail, i.e., high values. In Fig. 5c it can be seen that the nonstationary return levels capture the inter-annual variability of the observed precipitation extremes very well, in that, the return levels shift up and down in concert with the historical values. A similar or even better performance showed in Fig. 5 was seen at all the other stations.

Fig. 6 shows the conditional posterior median of the regression coefficients corresponding to the covariates for the location, shape, and scale parameters of GEV over the 0.5-degree grid from the 5000 simulations. The median of the intercept of the location parameter (Fig. 6a) shows higher values in the eastern part of the region and lower in the western. This is consistent with the climatology of the seasonal extreme precipitation (see Fig. 2) – in that the western parts are arid and semi-arid and hence lower precipitation. The conditional posterior median of SASP coefficients of the location (Fig. 6b) is higher in the east, and it is positive over most of the region with small negative regions in the middle of the domain. This can be explained by the orographic effect due to the presence of the mountain ranges. The conditional posterior median for the intercept of log of the scale parameter (Fig. 6c) also shows similar spatial variability as the intercept of the location, indicating that regions with higher extreme rainfall have higher variability. The conditional posterior median of SASP coefficients of log of the scale parameter (Fig. 6d) shows similar spatial variability as the SASP coefficients of the location, i.e., higher values in the east and regions with negative values in the middle of the domain. The conditional posterior median of the shape parameter (Fig. 6e) indicates heavy tail distribution (i.e. positive shape parameter) in the arid and semi-arid regions in the west part. However, its range of variation is small.

Fig. 7 shows the scatter plots of the conditional posterior spatial regression coefficients β_{0,α_1} (intercept of α_1) vs. β_{0,α_0} (longitude slope of

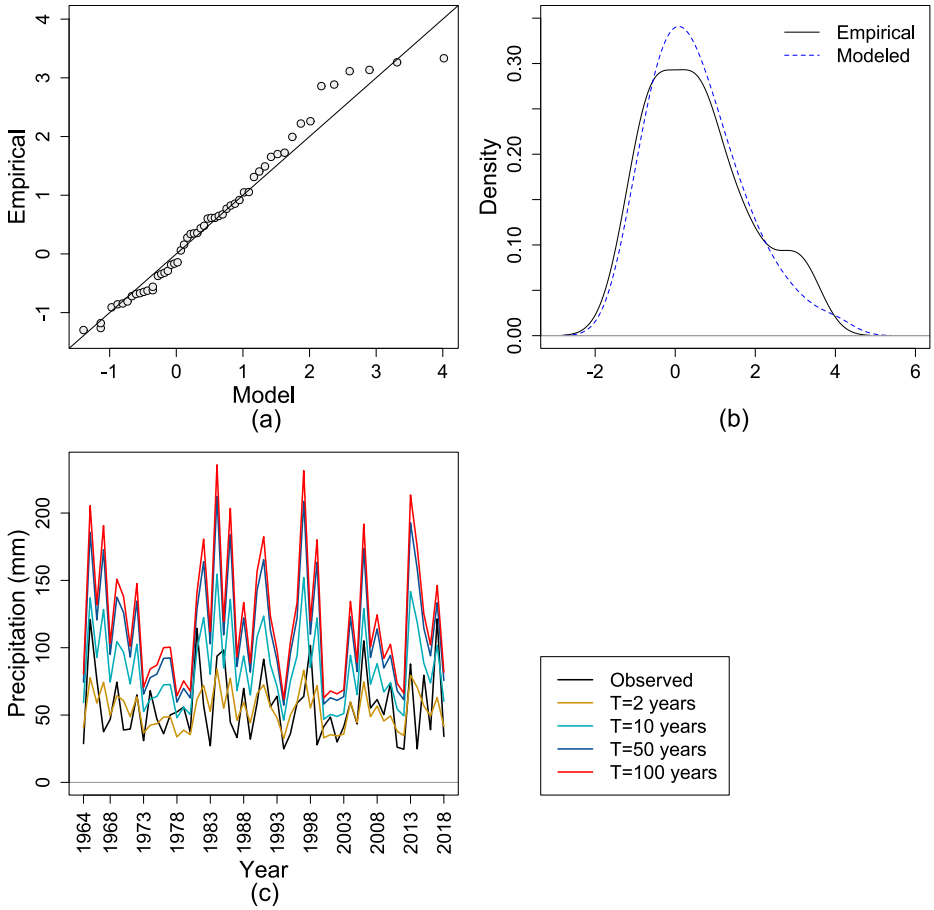

Fig. 5. (a) Q-Q plot , (b) PDF of the GEV distribution fitting, and (c) time series of nonstationary of the MLE return levels for different return periods for extreme summer precipitation at Pasamonte station, NM. In panel (b), the data are first transformed to an appropriate standardized GEV scale. The empirical PDF is obtained by a kernel density estimator. In panel (c), the black line corresponds to the observed.

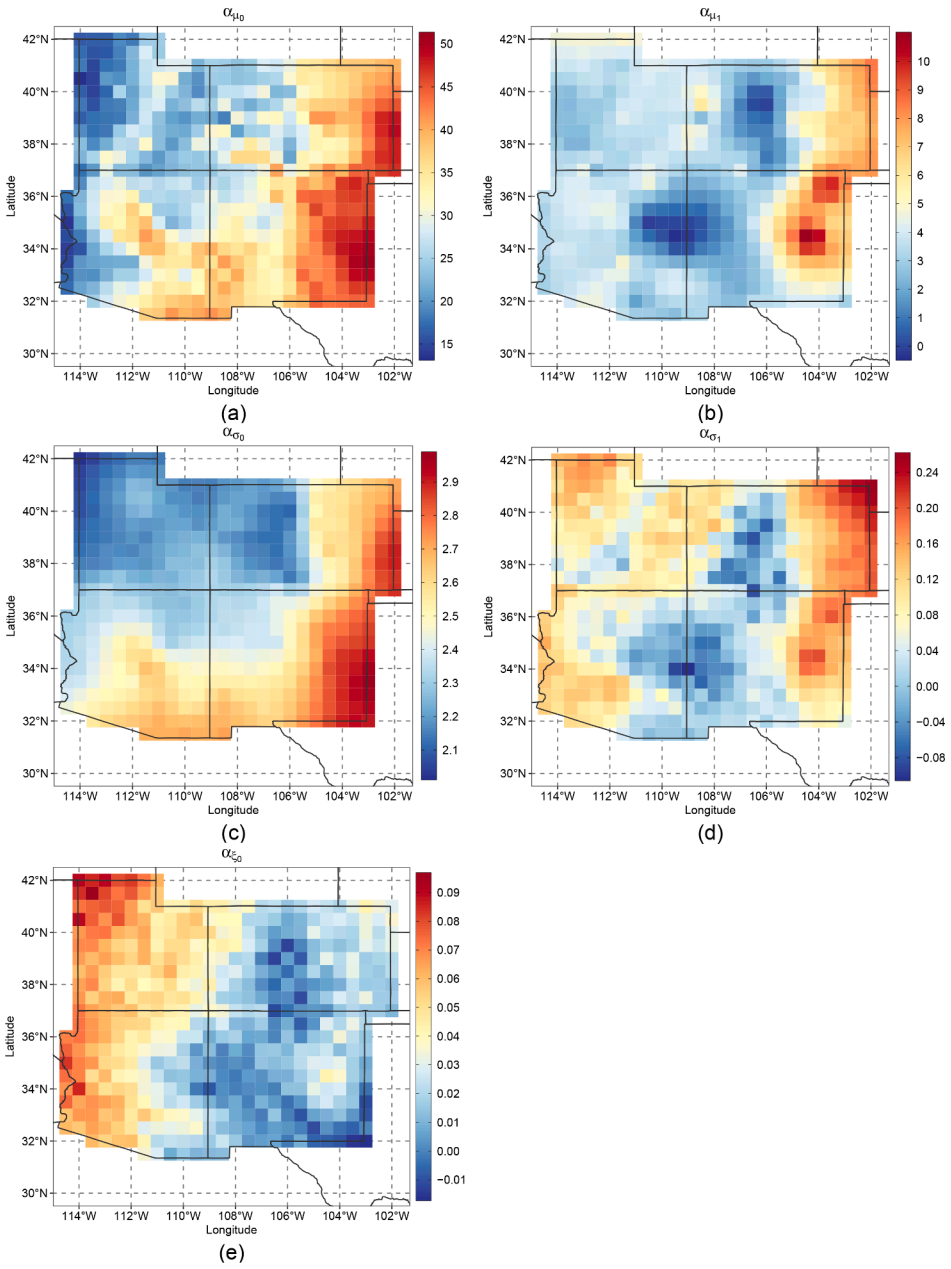

Fig. 6. The conditional posterior median of the regression coefficients of GEV parameters over a 0.5-degree grid: (a) intercept of the location parameter, $\boldsymbol{\alpha}_{\mu_0}$; (b) SASP coefficient of the location parameter, $\boldsymbol{\alpha}_{\mu_1}$; (c) intercept of the log of the scale parameter, $\boldsymbol{\alpha}_{\sigma_0}$; (d) SASP coefficient of the log of the scale parameter, $\boldsymbol{\alpha}_{\sigma_1}$; and (f) shape parameter, $\boldsymbol{\alpha}_{\xi_0}$.

α_1) for the semi-Bayesian univariate model (Fig. 7a) and semi-Bayesian multivariate model (Fig. 7b). It is seen that contrary to semi-Bayesian univariate model, semi-Bayesian multivariate model can capture the cross-correlation between spatial regression coefficients for different GEV regression coefficients even when we set up uncorrelated priors for them. The same feature was observed for other spatial regression coefficients.

The same feature is observed for the residuals. This is shown in Fig. 8 that displays Sample cross-variograms (for more details see Ver Hoef and Cressie, 1993) of $\boldsymbol{\alpha}_{\mu_0}$-$\boldsymbol{\alpha}_{\mu_1}$ from the predicted residuals obtained from the linear model fitting on the maximum likelihood estimates (MLE) of the GEV regression coefficients (Fig. 8a), the conditional posterior residuals obtained from the semi-Bayesian univariate model (Fig. 8b), and the conditional posterior residuals obtained from the semi-Bayesian multivariate model (Fig. 8c). Solid lines represent the least squares estimation of the exponential model of cross-variogram. It is seen that for semi-Bayesian multivariate case, posterior residuals can capture the spatial cross-correlation between the residuals observed for the MLE case, the observed residuals in our case. This feature is not captured by the semi-Bayesian univariate model again. The same was observed for $\boldsymbol{\alpha}_{\mu_0}$–$\boldsymbol{\alpha}_{\sigma_0}$ and $\boldsymbol{\alpha}_{\mu_1}$–$\boldsymbol{\alpha}_{\sigma_0}$.

Thus, by capturing cross-correlation between spatial coefficients and residuals with our framework is possible to obtain more consistent simulations of the GEV regression coefficients, and consequently, reduce the uncertainty of the extreme precipitation return levels estimates.

4.2. *Spatial variability of return levels*

To assess the ability of the model to capture the spatial patterns of the summer precipitation extremes, we present results of 2-year return levels along with the associated observations. Fig. 9 shows the spatial map of the conditional posterior median of the 2-year return level of

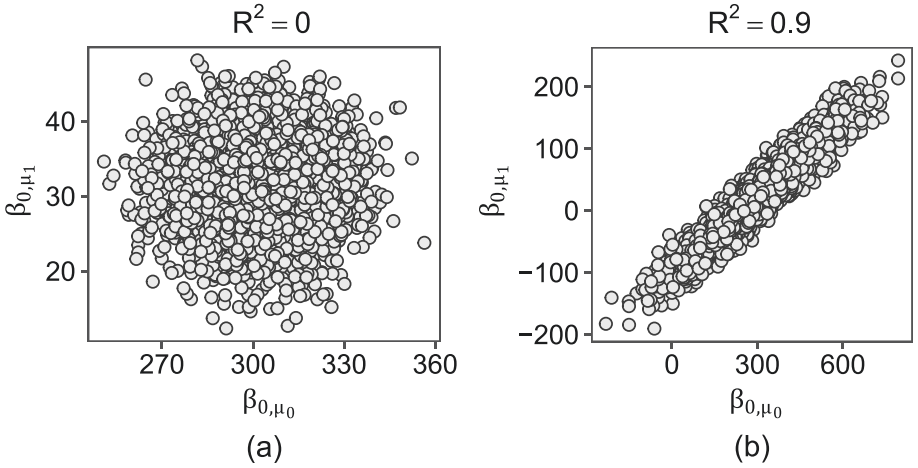

Fig. 7. Scatter plots of the conditional posterior spatial regression coefficients intercept of μ_1 vs. intercept of μ_0 for: (a) semi-Bayesian univariate model; (b) semi-Bayesian multivariate model. Correlation coefficient for the semi-Bayesian multivariate model is significant at a significance level of 0.01.

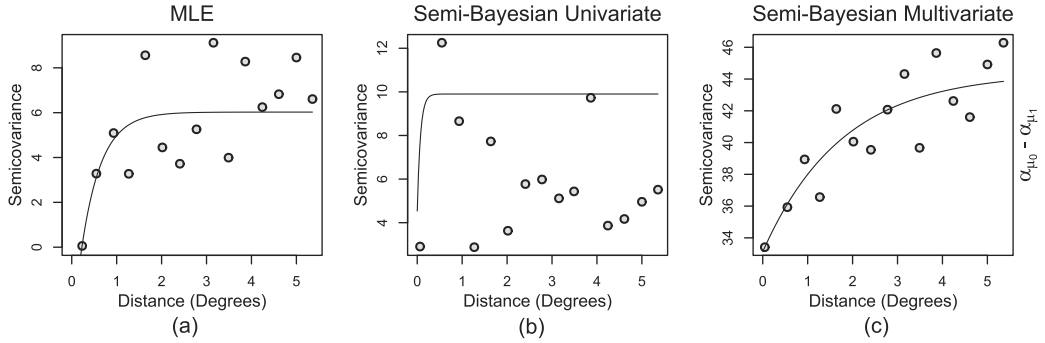

Fig. 8. Sample cross-variograms of $\boldsymbol{\alpha}_{\mu_0}$–$\boldsymbol{\alpha}_{\mu_1}$ from: (a) the predicted residuals obtained from the linear model fitting on the maximum likelihood estimates of the GEV regression coefficients; (b) the conditional posterior residuals obtained from the semi-Bayesian univariate model; (c) the posterior residuals obtained from the semi-Bayesian multivariate model. Solid lines represent the least squares estimation of the exponential model of the cross-variogram.

summer precipitation extremes along with the median of the observed extremes at the station locations and also for representative wet and dry years. Fig. 9a shows the conditional posterior median of the 2-year return level over all the years and the corresponding 95% credible interval width in Fig. 9b. The median of historical precipitation extremes at the stations – comparable to the posterior median of the 2-year return level - are shown in Fig. 9a as colored circles. It can be seen that the median values are lower in the arid and semi-arid western regions of the domain and higher in the eastern parts, which are consistent with the historical median values at the stations (the colors in the circles are consistent with that of the background from the simulations). The credible intervals widths do not show any spatial pattern. We selected a wet year (1997) in the record and show the conditional posterior median of the 2-year return level in Fig. 9c and the historical observed values at the stations are consistent with the simulations, more so in the western part of the domain. However, in the eastern part of the domain, with high precipitation, the simulations are slightly lower than the observations. The spatial pattern of the credible interval width (Fig. 9d) is similar to that in Fig. 9b. For a representative dry year (2001), the conditional posterior median of the 2-year return level and observed correspond very well (Fig. 9e) with a similar spatial pattern of credible interval width (Fig. 9f) to that of the simulations over the entire time domain (Fig. 9b).

Fig. 10 shows the conditional posterior median of the 100-year return level of summer precipitation extreme and its 95% confidence interval width. In Fig. 10a can be seen that this, too, shows a similar spatial pattern to that of the 2-year return level, i.e., higher precipitation in the east and lower in the west. This is consistent with the spatial pattern of the intercepts of the location and log of the scale parameters (see Fig. 6). As in the case of 2-year return levels, the credible intervals widths do not show any spatial pattern (Fig. 10b).

4.3. Temporal variability of return levels

To assess the performance of the temporal variability of the nonstationary framework, we compared them (semi-Bayesian multivariate model) to the return levels from the MLE estimates of the GEV coefficientes, which are consider as the true values in this case, and to those return levels from the semi-Bayesian univariate model. In Fig. 11 we show the boxplots of the nonstationary 100-year return level for each year at Pasamonte station, NM from the semi-Bayesian univariate model (Fig. 11a) and the framework proposed here (semi-Bayesian multivariate, Fig. 11b) along with those from the MLE estimates of the GEV coefficients (red line). The whiskers show the 95% credible intervals, the boxes the interquartile range, and the horizontal lines inside the boxes, the median. The nonstationary framework proposed here shows a significant reduction in the uncertainty compared to the semi-Bayesian univariate model. This can be explained by the ability of the framework proposed here to capture the cross-correlation between the spatial regression coefficients and between the spatial residuals (see Figs. 7 and 8). So, this allow to preserve the cross-correlation at site of MLE estimates of the GEV regression coefficients for each simulation of the coefficients.

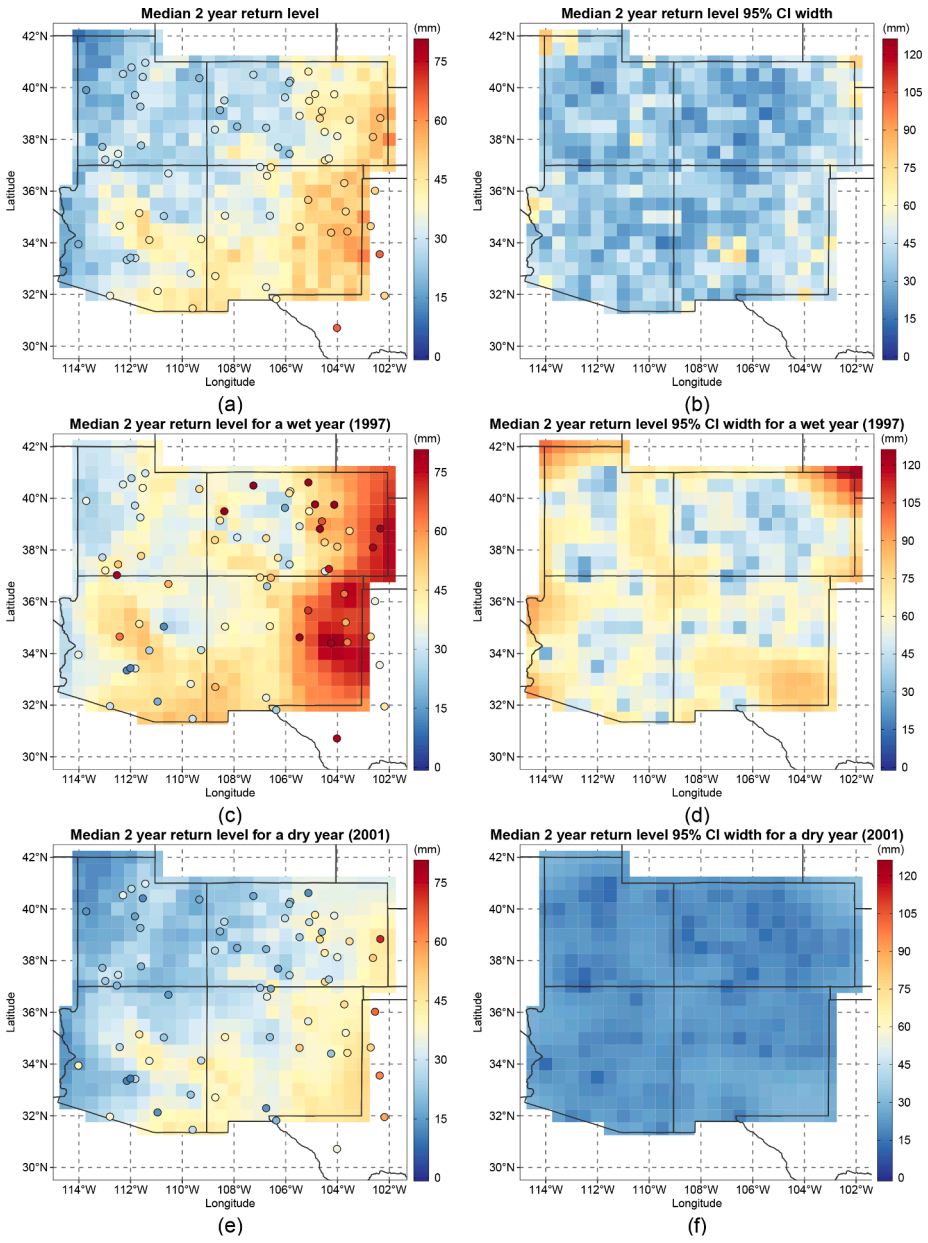

Fig. 9. Conditional posterior median 2-year return level of extreme summer precipitation and the corresponding 95% confidence interval width for the whole record (a and b), a wet year (1997, c and d), a dry year (2001, e and f). Points in panels (a), (b), and (c) correspond to the median of the observed for the whole record, and the observed for wet and dry years, respectively.

4.4. Cross-validation

To test the out-of-sample predictability of the model, cross-validation was carried out by dropping 10% of the total stations (i.e., 7 out of 73 stations), and the model was fit on the remaining 66 stations. Stations dropped are shown in Fig. 12 (red circles), and were chosen to represent distinct climatological behaviors, as well as geographical sampling. To quantify the skill in a prediction mode, we made two different predictions: at the dropped stations and spatial validations. First, we predict the distributions at the dropped stations, and randomly generated 5000 samples of extreme precipitation values at the dropped locations for each year. In this case, we created boxplots for the 7 stations dropped for the validation model dropping 10% of the data (subset data model) and observed data. Next, we generated predictive posterior distributions over the 0.5-degreed grid using this model based on subset data (66 stations), and subsequently, generated 5000 samples of 100-year returns level over the same grid according to the Section 3.5. We computed the difference between the median return level from the full data model (Fig. 10) and this subset data model. .

Fig. 13 shows predicted summer precipitation extremes for the period (1964–2018) at stations dropped for the validation model dropping 10% of the data for the semi-Bayesian univariate model (light gray boxes), semi-Bayesian multivariate model (gray boxes) and the observed data (yellow boxes). The distribution from the semi-Bayesian multivariate model captures the historical distribution quite well as the box and whiskers are comparable between the two, indicating acceptable predictability, offering prospects for this approach to be used in a predictive mode. Also, it shows a better performance in capturing the historical distribution than the semi-Bayesian univariate model and a lower uncertainty. Overall, the same feature is seen for dry (2001) and wet (1997) year cases (Fig. 14). Station 5 shows the worst performance, but in general, the performance is acceptable for almost all the station (yellow circles fall into the boxes).

Fig. 15 shows the difference between the conditional posterior

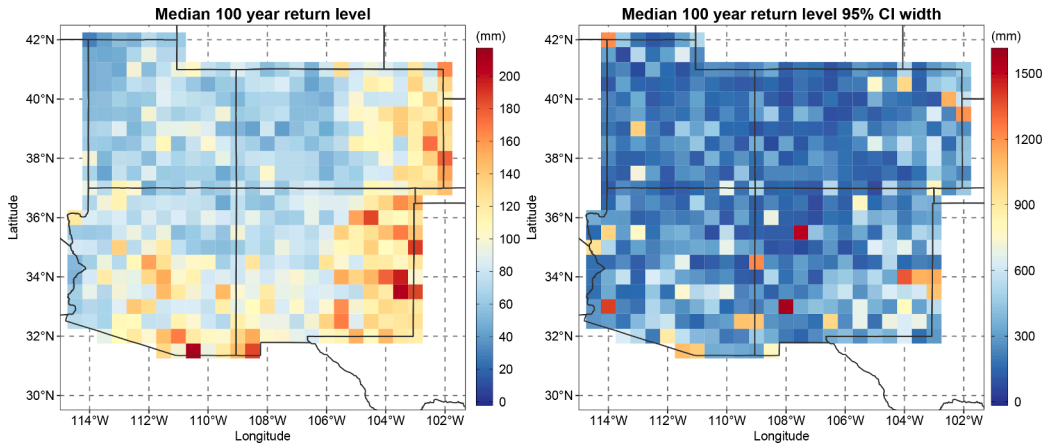

Fig. 10. Conditional posterior median 100-year return level of extreme summer precipitation along with the median of the observed (left) and median 100-year return level of 95% confidence interval width of extreme summer precipitation (right).

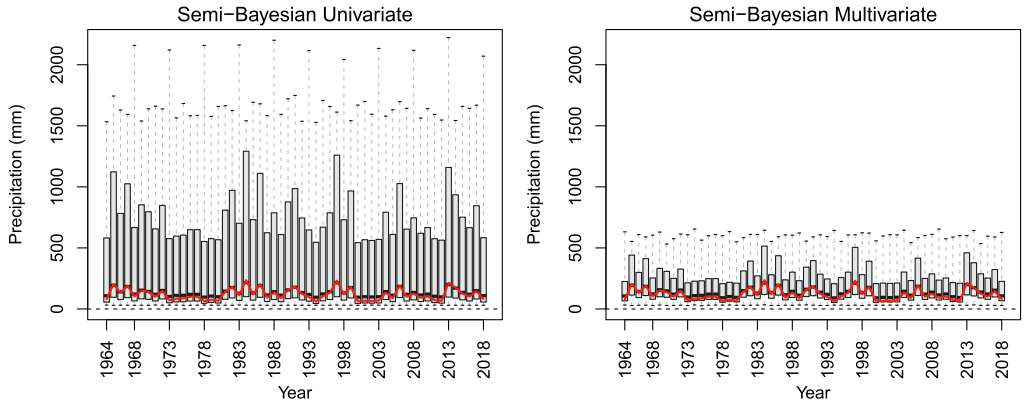

Fig. 11. Nonstationary 100-year return levels from (a) the semi-Bayesian univariate model (b) the semi-Bayesian multivariate model of extreme summer precipitation at Pasamonte station, NM. Red line corresponds to the nonstationary 100-year return levels from the MLE estimates of the GEV regression coefficients. (For interpretation of the references to colour in this figure legend, the reader is referred to the web version of this article.)

median 100-year return levels from the full data model and the subset data model over the 0.5-degree grid. In general, the difference map does not show spatial patterns except for a bias in the south of Arizona. This bias can be caused by poor data in this region and that two of the stations dropped (stations 3 and 6) are located in this region. However, the differences are not high compared to the magnitude of 100-year return levels (Fig. 10), so the performance of the model could be considered well.

5. Summary and discussion

In this study, we presented a spatial–temporal multivariate semi-Bayesian hierarchical framework for conducting nonstationary frequency analysis of precipitation extremes at ungauged locations. The framework assumes the marginal distribution of each location is a generalized extreme value (GEV) distribution, where the distribution parameters can vary in time as a function of covariates, whose coefficients are estimated via maximum likelihood. To get estimates at ungauged locations or over a grid, the spatial dependence is captured by modeling spatially the coefficients of the covariates at each station using spatial Gaussian multivariate processes.

We applied this framework to conduct nonstationary frequency analysis of extreme summer precipitation at 73 stations from the Southwest US. This application incorporated large-scale climate indexes such as ENSO and PDO and the standardized spatial average of summer seasonal precipitation (SASP) over the region as potential covariates. Based on the lowest total AIC and BIC, we selected the best model which only considers SASP as covariate for the location and scale paremeters, and stationary shape parameter. We found that the multivariate semi-Bayesian approach can capture the cross-correlation between the spatial regression coefficients and the residuals, provided a robust estimation of uncertainties of the return levels due to the spatial interpolation compared to univariate semi-Bayesian model, and capture the spatial patterns of the observed data.

In the application presented here, we only considered three potential covariates, and the shape parameter was assumed to be stationary for simplicity. However, Additional Skillful covariates can further improve the estimates of space–time variability. In the case of that, the framework can be applied to a local scale, and local covariates can be included to capture well local patterns.

The spatial modeling of the process level parameters by incorporating correlation among the parameters makes a new contribution. Besides, this correlation enables to reduce the parameter uncertainty related to the spatial interpolation. We recognize that the uncertainty captured by our model does not represent the total uncertainty, as we are employing the Bayesian framework on the ML estimates of the GEV coefficients. The uncertainty in the ML estimates is not captured explicitly. Of course, one could include this estimation in the first layer, inside of the Bayesian framework, to capture this additional uncertainty. However, over a large spatial domain such as the Southwest U.S., this makes the model computationally intensive and with no guarantees of convergence. The semi-Bayesian model presented here, makes this tradeoff to enable an efficient model capture most of the uncertainties. A fully Bayesian framework with efficient computational methods will be

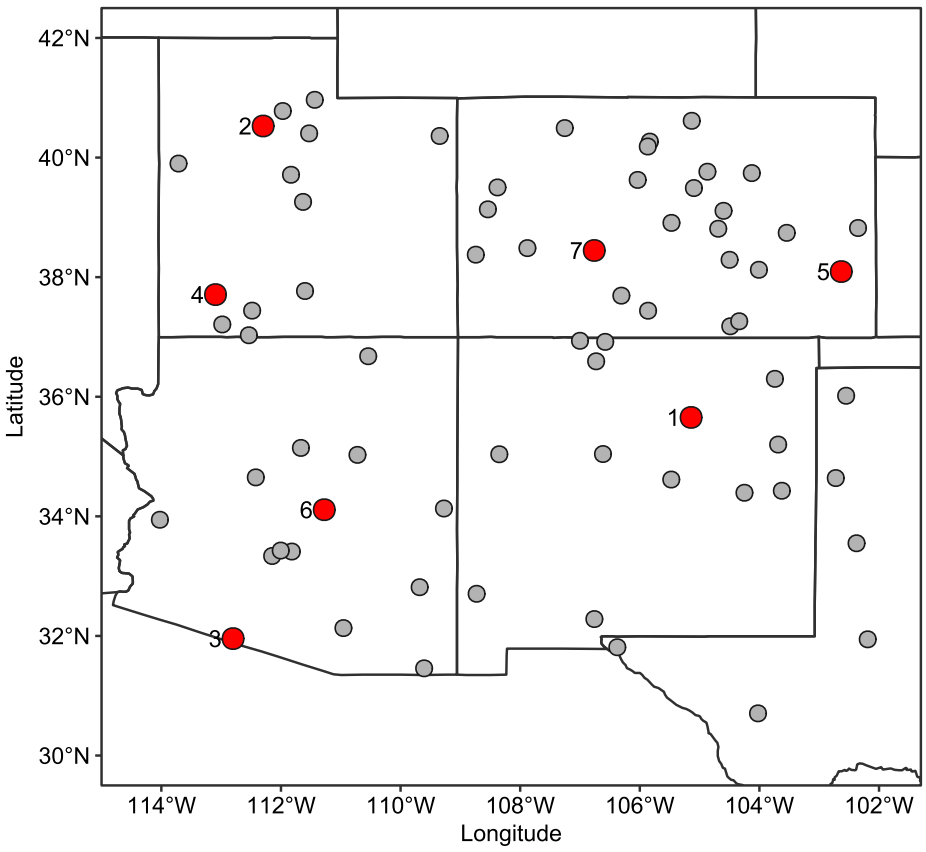

Fig. 12. stations dropped (7) for the cross-validation (red circles) and the subset data (66 stations) using to fit the model (gray circles). (For interpretation of the references to colour in this figure legend, the reader is referred to the web version of this article.)

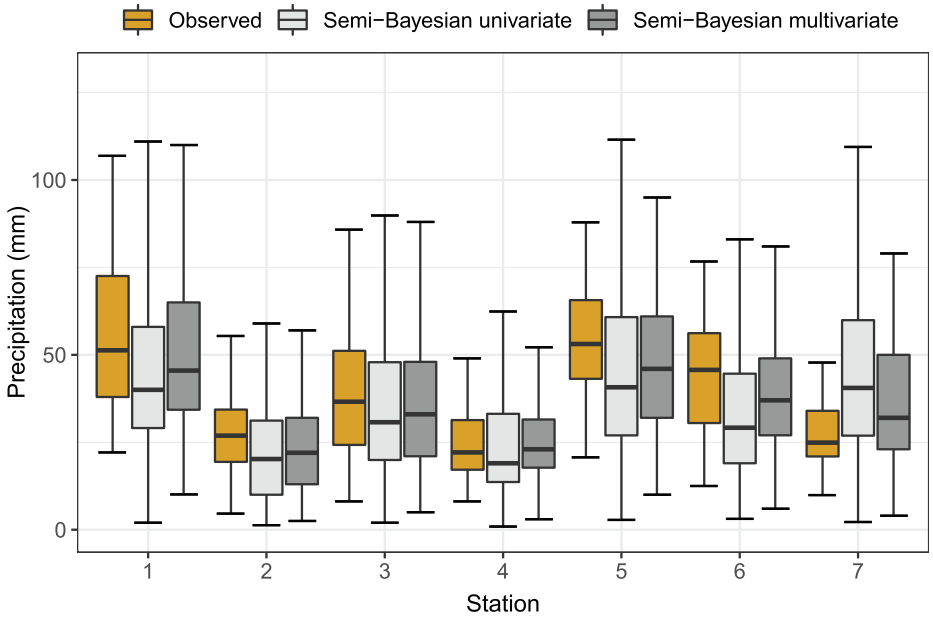

Fig. 13. Predicted extreme summer precipitation (1964–2018) at 10% random leave-out stations for the validation model dropping 10% of the data for the semi-Bayesian univariate model (light gray boxes), semi-Bayesian multivariate model (gray boxes), and observed data (yellow boxes). The whiskers show the 95% credible intervals, the boxes the interquartile range, and the horizontal lines inside the boxes, the median. (For interpretation of the references to colour in this figure legend, the reader is referred to the web version of this article.)

a natural extension.

The model performance skill will be dependent on the strength of the temporal covariates in their association with the variability of the extremes field. In the application here, we were motivated by our ongoing research on the summer precipitation over southwest US. It is generally known that the summer precipitation and the extremes in this region exhibits high degree of variability and weaker connection with large scale forcings compared to their winter counterpart. However, the user can develop tailored covariates to their application. If the covariates are lagged in time (say a season head), this modeling framework can be used to provide projections of seasonal extremes that will be of help in operational planning and management of natural resources ahead of the active season of extremes. Furthermore, with multi-decadal projections of the covariates, say under a global warming scenarios, projections of

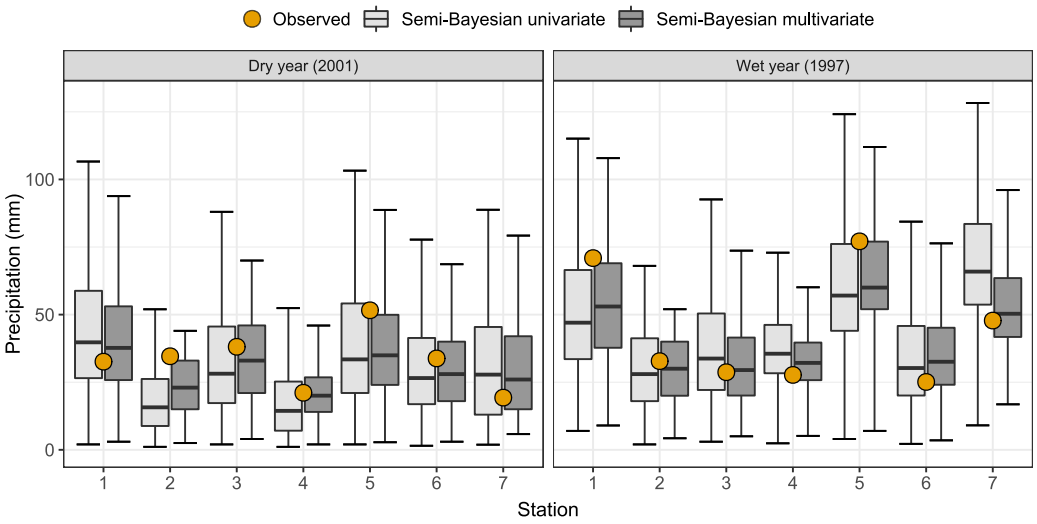

Fig. 14. Predicted extreme summer precipitation for a dry (2001, left) and a wet (1997, right) year at 10% random leave-out stations for the validation model dropping 10% of the data for the semi-Bayesian univariate model (light gray boxes), semi-Bayesian multivariate model (gray boxes), and the observed data (yellow circles). The whiskers show the 95% credible intervals, the boxes the interquartile range, and the horizontal lines inside the boxes, the median. (For interpretation of the references to colour in this figure legend, the reader is referred to the web version of this article.)

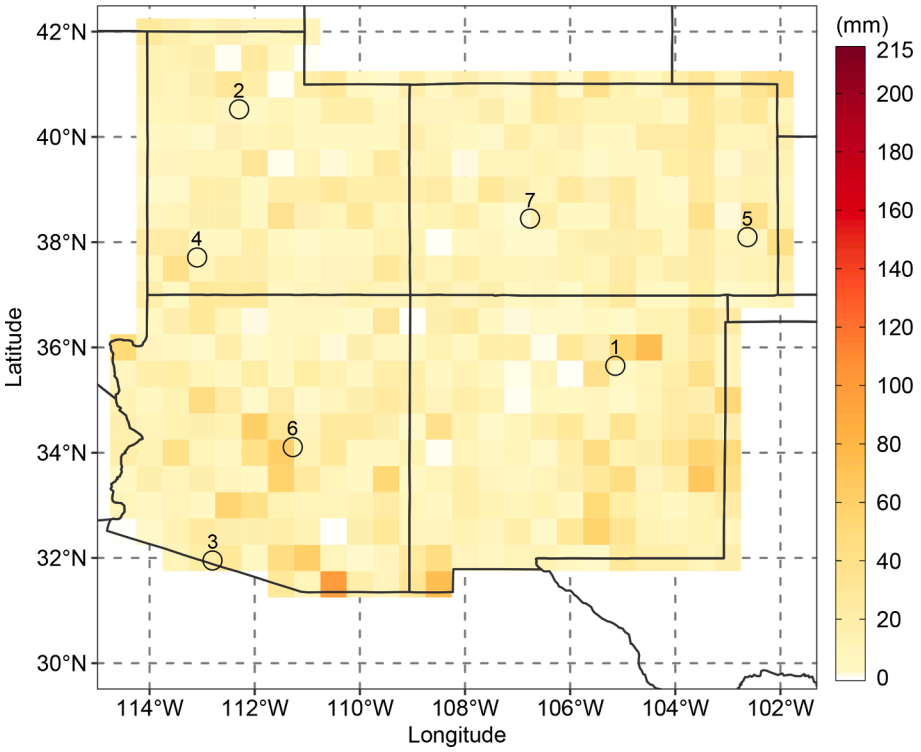

Fig. 15. Difference between conditional posterior median return 100-year return levels from the full model and the validation model dropping 10% of the data over the 0.5-degree grid. Circles correspond to the stations dropped (7) for the cross-validation. Note the scale keeps the upper limit of the median 100-year return level of extreme summer precipitation (Fig. 10).

climate extremes for these scenarios can be made, for use by policy makers. Extensions of this framework to other fields of extremes such as streamflow, temperature, pollution concentrations in space etc., and to threshold exceedances, can be easily enabled.

CRediT authorship contribution statement

Álvaro Ossandón: Conceptualization, Methodology, Software, Validation, Formal analysis, Investigation, Resources, Writing - original draft, Visualization, Funding acquisition. **Balaji Rajagopalan:** Conceptualization, Methodology, Investigation, Writing - review & editing, Supervision, Project administration, Funding acquisition. **William Kleiber:** Methodology, Writing - review & editing, Supervision, Funding acquisition.

Declaration of Competing Interest

The authors declare that they have no known competing financial interests or personal relationships that could have appeared to influence the work reported in this paper.

Acknowledgments

This project was funded by the National Science Foundation grant 1243270. We also acknowledge the support from a Fulbright fellowship and the National Agency for Research and Development (ANID)

Scholarship Program/

DOCTORADO BECAS CHILE/2015–56150013 for the first author. Partial support from the Monsoon Mission Project of the Ministry of Earth Sciences, India, for second author is thankfully acknowledged. The third author was supported by NSF DMS-1811294 and DMS-1923062. Analysis was conducted using the R language (R Core Team, 2017). Precipitation data were downloaded from the Global Historical Climatology Network https://www1.ncdc.noaa.gov/pub/data/ghcn/daily/. The MEI index is downloaded from the National Oceanic and Atmospheric Administration (NOAA) Earth Systems Research Laboratory (ESRL) Physical Sciences Division http://www.esrl.noaa.gov/psd/enso/mei/. The PDO index is available from the University of Washington http://research.jisao.washington.edu/pdo/. The elevation data were downloaded from the NASA Land Data Assimilation Systems https://ldas.gsfc.nasa.gov/nldas/elevation.

Appendix A. Abbreviations and acronyms

PDF	Probability Density Function
GEV	Generalized extreme value
ML	Maximum likelihood
MLE	Maximum likelihood estimates
AIC	Akaike information criteria
BIC	Bayesian information criterion
MCMC	Markov Chain Monte Carlo
GHCN	Global Historical Climatology Network
ENSO	El Nino Southern Oscillation
PDO	Pacific Decadal Oscillation
AMO	Atlantic Multidecadal Oscillation
SASP	Standardized spatial average of summer seasonal precipitation
MEI	Multivariate ENSO Index
NLDAS	NASA Land Data Assimilation Systems

References

Agilan, V., Umamahesh, N.V., 2016. Is the covariate based non-stationary rainfall IDF curve capable of encompassing future rainfall changes? J. Hydrol. 541, 1441–1455. https://doi.org/10.1016/j.jhydrol.2016.08.052.

Agilan, V., Umamahesh, N.V., 2017. What are the best covariates for developing non-stationary rainfall Intensity-Duration-Frequency relationship? Adv. Water Resour. 101, 11–22. https://doi.org/10.1016/j.advwatres.2016.12.016.

Ahn, K.-H., Palmer, R., Steinschneider, S., 2017. A hierarchical Bayesian model for regionalized seasonal forecasts: Application to low flows in the northeastern United States. Water Resour. Res. 53, 503–521. https://doi.org/10.1002/2016WR019605.

Akaike, H., 1974. A New Look at the Statistical Model Identification. IEEE Trans. Autom. Control 19, 716–723. https://doi.org/10.1109/TAC.1974.1100705.

Apanasovich, T.V., Genton, M.G., Sun, Y., 2012. A Valid Matérn Class of Cross-Covariance Functions for Multivariate Random Fields With Any Number of Components. J. Am. Stat. Assoc. 107, 180–193. https://doi.org/10.1080/01621459.2011.643197.

Apputhurai, P., Stephenson, A.G., 2013. Spatiotemporal hierarchical modelling of extreme precipitation in Western Australia using anisotropic Gaussian random fields. Environ. Ecol. Stat. 20, 667–677. https://doi.org/10.1007/s10651-013-0240-9.

Atyeo, J., Walshaw, D., 2012. A region-based hierarchical model for extreme rainfall over the UK, incorporating spatial dependence and temporal trend. Environmetrics 23, 509–521. https://doi.org/10.1002/env.2155.

Banerjee, S., Carilin, B.P., Gelfand, A.E., 2004. Modeling and Analysis for Spatial Data. CRC Press, Boca Raton.

Barnett, D.N., Brown, S.J., Murphy, J.M., Sexton, D.M., Webb, M.J., 2006. Quantifying uncertainty in changes in extreme event frequency in response to doubled CO2 using a large ensemble of GCM simulations. Clim. Dyn. 26, 489–511. https://doi.org/10.1007/s00382-005-0097-1.

Bowman, A.W., Azzalini, A., 1997. Applied smoothing techniques for data analysis: the kernel approach with S-Plus illustrations. Clarendon Press.

Bracken, C., Rajagopalan, B., Cheng, L., Kleiber, W., Gangopadhyay, S., 2016. Spatial Bayesian hierarchical modeling of precipitation extremes over a large domain. Water Resour. Res. 52, 6643–6655. https://doi.org/10.1002/2016WR018768. arXiv:1512.08560.

Bracken, C., Holman, K.D., Rajagopalan, B., Moradkhani, H., 2018. A Bayesian Hierarchical Approach to Multivariate Nonstationary Hydrologic Frequency Analysis. Water Resour. Res. 54, 243–255. https://doi.org/10.1002/2017WR020403.

Cannon, A.J., 2010. A flexible nonlinear modelling framework for nonstationary generalized extreme value analysis in hydroclimatology. Hydrol. Process. 24, 673–685. https://doi.org/10.1002/hyp.7506.

Cheng, L., Aghakouchak, A., 2014. Nonstationary precipitation intensity-duration-frequency curves for infrastructure design in a changing climate. Sci. Rep. 4, 1–6. https://doi.org/10.1038/srep07093.

Cheng, L., Aghakouchak, A., Gilleland, E., Katz, R.W., 2014. Non-stationary extreme value analysis in a changing climate. Clim. Change 127, 353–369. https://doi.org/10.1007/s10584-014-1254-5.

Coles, S.G., 1993. Regional Modelling of Extreme Storms Via Max-Stable Processes. J. Roy. Stat. Soc.: Ser. B (Methodol.) 55, 797–816. https://doi.org/10.1111/j.2517-6161.1993.tb01941.x.

Coles, S., 2001. An introduction to statistical modeling of extreme values. Springer, London, UK.

Coles, S.G., Tawn, J.A., 1996. Modelling Extremes of the Areal Rainfall Process. J. Roy. Stat. Soc.: Ser. B (Methodol.) 58, 329–347. https://doi.org/10.1111/j.2517-6161.1996.tb02085.x.

Cooley, D., Sain, S.R., 2010. Spatial hierarchical modeling of precipitation extremes from a regional climate model. J. Agric. Biol. Environ. Stat. 15, 381–402. https://doi.org/10.1007/s13253-010-0023-9.

Cooley, D., Nychka, D., Naveau, P., 2007. Bayesian spatial modeling of extreme precipitation return levels. J. Am. Stat. Assoc. 102, 824–840. https://doi.org/10.1198/016214506000000780.

Cressie, N. A. C. 1993. Statistics for Spatial Data, volume 15 of Wiley Series in Probability and Statistics, John Wiley & Sons, Inc., Hoboken, NJ, USA. doi: 10.1002/9781119115151.

Davison, A.C., Padoan, S.A., Ribatet, M., 2012. Statistical modeling of spatial extremes. Stat. Sci. 27, 161–186. https://doi.org/10.1214/11-STS376.

Dupuis, D.J., Field, C.A., 1998. Robust estimation of extremes. Can. J. Stat. 26, 199–215. https://doi.org/10.2307/3315505.

Dyrrdal, A.V., Lenkoski, A., Thorarinsdottir, T.L., Stordal, F., 2015. Bayesian hierarchical modeling of extreme hourly precipitation in Norway. Environmetrics 26, 89–106. https://doi.org/10.1002/env.2301. arXiv:1309.6111.

El Adlouni, S., Ouarda, T.B., Zhang, X., Roy, R., Bobée, B., 2007. Generalized maximum likelihood estimators for the nonstationary generalized extreme value model. Water Resour. Res. 43 https://doi.org/10.1029/2005WR004545.

Finley, A.O., Banerjee, S., Gelfand, A.E., 2015. spBayes for large univariate and multivariate point-referenced spatio-temporal data models. J. Stat. Softw. 63, 1–28. https://doi.org/10.18637/jss.v063.i13.

Fowler, H.J., Cooley, D., Sain, S.R., Thurston, M., 2010. Detecting change in UK extreme precipitation using results from the climateprediction.net BBC climate change experiment. Extremes 13, 241–267. https://doi.org/10.1007/s10687-010-0101-y.

Frich, P., Alexander, L., Della-Marta, P., Gleason, B., Haylock, M., Klein Tank, A., Peterson, T., 2002. Observed coherent changes in climatic extremes during the second half of the twentieth century. Clim. Res. 19, 193–212. https://doi.org/10.3354/cr019193.

Gao, M., Mo, D., Wu, X., 2016. Nonstationary modeling of extreme precipitation in China. Atmos. Res. 182, 1–9. https://doi.org/10.1016/j.atmosres.2016.07.014.

Gellens, D., 2002. Combining regional approach and data extension procedure for assessing GEV distribution of extreme precipitation in Belgium. J. Hydrol. 268, 113–126. https://doi.org/10.1016/S0022-1694(02)00160-9.

Gilleland, E., Katz, R.W., 2016. ExtRemes 2.0: An extreme value analysis package in R. J. Stat. Softw. 72, 1–39. https://doi.org/10.18637/jss.v072.i08.
Gneiting, T., Kleiber, W., Schlather, M., 2010. Matérn Cross-Covariance Functions for Multivariate Random Fields. J. Am. Stat. Assoc. 105, 1167–1177. https://doi.org/10.1198/jasa.2010.tm09420.
Hanel, M., Buishand, T.A., Ferro, C.A.T., 2009. A nonstationary index flood model for precipitation extremes in transient regional climate model simulations. J. Geophys. Res. 114, D15107. https://doi.org/10.1029/2009JD011712.
Hershfield, D.M. 1961. Rainfall Frequency Atlas of the United States for Durations from 30 Minutes to 24 Hours and Return Periods from I to 100 Years, Technical Report, U. S. Weather Bureau, Washington, D.C.
Higgins, R.W., Chen, Y., Douglas, A.V., 1999. Interannual Variability of the North American Warm Season Precipitation Regime. J. Clim. 12, 653–680. https://doi.org/10.1175/1520-0442(1999)012<0653:IVOTNA>2.0.CO;2.
IPCC, 2007. Climate change 2007: the physical science basis, Technical Report, New York.
Jakob, D. 2013. Nonstationarity in extremes and engineering design, in: A. AghaKouchak, D. Easterling, K. Hsu, S. Schubert, S. Sorooshian (Eds.), Extremes in a Changing Climate, volume 65 of Water Science and Technology Library, Springer, Dordrecht, 2013, pp. 363–417. doi:10.1007/978-94-007-4479-0.
Katz, R.W., 2013. Statistical Methods for Nonstationary Extremes. In: AghaKouchak, A., Easterling, D., Hsu, K., Schubert, S., Sorooshian, S. (Eds.), Extremes in a Changing Climate, 65 ed. Springer, Dordrecht, pp. 15–37.
Katz, R.W., Parlange, M.B., Naveau, P., 2002. Statistics of extremes in hydrology. Adv. Water Resour. 25, 1287–1304. https://doi.org/10.1016/S0309-1708(02)00056-8.
Lima, C.H., Lall, U., Troy, T., Devineni, N., 2016. A hierarchical Bayesian GEV model for improving local and regional flood quantile estimates. J. Hydrol. 541, 816–823. https://doi.org/10.1016/j.jhydrol.2016.07.042.
Mamalakis, A., Yu, J.Y., Randerson, J.T., Aghakouchak, A., Foufoula-Georgiou, E., 2018. A new interhemispheric teleconnection increases predictability of winter precipitation in southwestern US. Nat. Commun. 9, 1–10. https://doi.org/10.1038/s41467-018-04722-7.
McCabe, G.J., Palecki, M.A., Betancourt, J.L., 2004. Pacific and Atlantic Ocean influences on multidecadal drought frequency in the United States. Proc. Natl. Acad. Sci. USA 101, 4136–4141. https://doi.org/10.1073/pnas.0306738101.
McCullagh, P., Nelder, J.A., 1989. Generalized Linear Models, Second Edition. Taylor & Francis.
Menne, M.J., Durre, I., Vose, R.S., Gleason, B.E., Houston, T.G., 2012. An overview of the global historical climatology network-daily database. J. Atmos. Oceanic Technol. 29, 897–910. https://doi.org/10.1175/JTECH-D-11-00103.1.
Milly, P.C.D., Betancourt, J., Falkenmark, M., Hirsch, R.M., Kundzewicz, Z.W., Lettenmaier, D.P., Stouffer, R.J. 2008. Stationarity Is Dead: Whither Water Management? Science 319, 573 LP – 574. doi: 10.1126/science.1151915.
Ouarda, T., El-Adlouni, S., 2011. Bayesian nonstationary frequency analysis of hydrological variables. J. Am. Water Resour. Assoc. 47, 496–505. https://doi.org/10.1111/j.1752-1688.2011.00544.x.
R Core Team, 2017. R: A Language and Environment for Statistical Computing, R Foundation for Statistical Computing, Vienna, Austria.
Read, L.K., Vogel, R.M., 2015. Reliability, return periods, and risk under nonstationarity. Water Resour. Res. 51, 6381–6398. https://doi.org/10.1002/2015WR017089.
Renard, B., 2011. A Bayesian hierarchical approach to regional frequency analysis. Water Resour. Res. 47 https://doi.org/10.1029/2010WR010089.
Reza Najafi, M., Moradkhani, H., 2013. Analysis of runoff extremes using spatial hierarchical Bayesian modeling. Water Resour. Res. 49, 6656–6670. https://doi.org/10.1002/wrcr.20381.
Robert, C. P., Casella, G., 2004. Monte Carlo Statistical Methods, Springer Texts in Statistics, Springer, New York, NY. doi: 10.1007/978-1-4757-4145-2.
Salas, J.D., Obeysekera, J., 2014. Revisiting the Concepts of Return Period and Risk for Nonstationary Hydrologic Extreme Events. J. Hydrol. Eng. 19, 554–568. https://doi.org/10.1061/(ASCE)HE.1943-5584.0000820.
Schmidli, J., Frei, C., 2005. Trends of heavy precipitation and wet and dry spells in Switzerland during the 20th century. Int. J. Climatol. 25, 753–771. https://doi.org/10.1002/joc.1179.
Schwarz, G., 1978. Estimating the Dimension of a Model. Ann. Stat. 6, 461–464. https://doi.org/10.2307/2958889.
Sheppard, P.R., Comrie, A.C., Packin, G.D., Angersbach, K., Hughes, M.K., 2002. The climate of the US Southwest. Clim. Res. 21, 219–238.
Steinschneider, S., Lall, U., 2015. A hierarchical Bayesian regional model for nonstationary precipitation extremes in Northern California conditioned on tropical moisture exports. Water Resour. Res. 51, 1472–1492. https://doi.org/10.1002/2014WR016664.
Stephenson, A.G., Lehmann, E.A., Phatak, A., 2016. A max-stable process model for rainfall extremes at different accumulation durations. Weather Clim. Extrem. 13, 44–53. https://doi.org/10.1016/j.wace.2016.07.002.
Sun, X., Thyer, M., Renard, B., Lang, M., 2014. A general regional frequency analysis framework for quantifying local-scale climate effects: A case study of ENSO effects on Southeast Queensland rainfall. J. Hydrol. 512, 53–68. https://doi.org/10.1016/j.jhydrol.2014.02.025.
Um, M.J., Kim, Y., Markus, M., Wuebbles, D.J., 2017. Modeling nonstationary extreme value distributions with nonlinear functions: An application using multiple precipitation projections for U.S. cities. J. Hydrol. 552, 396–406. https://doi.org/10.1016/j.jhydrol.2017.07.007.
van Haren, R., van Oldenborgh, G.J., Lenderink, G., Hazeleger, W., 2013. Evaluation of modeled changes in extreme precipitation in Europe and the Rhine basin. Environ. Res. Lett. 8, 14053. https://doi.org/10.1088/1748-9326/8/1/014053.
Vasiliades, L., Galiatsatou, P., Loukas, A., 2015. Nonstationary Frequency Analysis of Annual Maximum Rainfall Using Climate Covariates. Water Resour. Manage 29, 339–358. https://doi.org/10.1007/s11269-014-0761-5.
Ver Hoef, J.M., Cressie, N., 1993. Multivariable spatial prediction. Math. Geol. 25, 219–240. https://doi.org/10.1007/BF00893273.
Wazneh, H., Chebana, F., Ouarda, T.B.M.J., 2013. Depth-based regional index-flood model. Water Resour. Res. 49, 7957–7972. https://doi.org/10.1002/2013WR013523.
Wilks, D.S., 1993. Comparison of three-parameter probability distributions for representing annual extreme and partial duration precipitation series. Water Resour. Res. 29, 3543–3549. https://doi.org/10.1029/93WR01710.
Wolter, K., and Timlin, M. S., 1993. Monitoring ENSO in COADS with a seasonally adjusted principal component index, in: The 17th Climate Diagnostics, Norman, OK.
Wolter, K., Timlin, M.S., 1998. Measuring the strength of ENSO events: How does 1997/98 rank? Weather 53, 315–324. https://doi.org/10.1002/j.1477-8696.1998.tb06408.x.
Wolter, K., Timlin, M.S., 2011. El Niño/Southern Oscillation behaviour since 1871 as diagnosed in an extended multivariate ENSO index (MEI.ext). Int. J. Climatol. 31, 1074–1087. https://doi.org/10.1002/joc.2336.
Xia, Y., Mitchell, K., Ek, M., Sheffield, J., Cosgrove, B., Wood, E., Luo, L., Alonge, C., Wei, H., Meng, J., Livneh, B., Lettenmaier, D., Koren, V., Duan, Q., Mo, K., Fan, Y., Mocko, D., 2012. Continental-scale water and energy flux analysis and validation for the North American Land Data Assimilation System project phase 2 (NLDAS-2): 1. Intercomparison and application of model products. J. Geophys. Res.: Atmos. 117 https://doi.org/10.1029/2011JD016048.
Yan, H., Moradkhani, H., 2015. A regional Bayesian hierarchical model for flood frequency analysis. Stoch. Env. Res. Risk Assess. 29, 1019–1036. https://doi.org/10.1007/s00477-014-0975-3.
Yan, H., Moradkhani, H., 2016. Toward more robust extreme flood prediction by Bayesian hierarchical and multimodeling. Nat. Hazards 81, 203–225. https://doi.org/10.1007/s11069-015-2070-6.
Zhang, Y., Wallace, J.M., Battisti, D.S., 1997. ENSO-like Interdecadal Variability: 1900–93. J. Clim. 10, 1004–1020. https://doi.org/10.1175/1520-0442(1997)010<1004:ELIV>2.0.CO;2.